Erosion and Sediment Yields in the Changing Environment (Proceedings of a symposium held at the Institute of Mountain Hazards and Environment, CAS-Chengdu, China, 11–15 October 2012) (IAHS Publ. 356, 2012).

Quantification and modelling of debris flows in the proglacial area of the Gepatschferner, Austria, using ground-based LiDAR

FLORIAN HAAS, TOBIAS HECKMANN, LUDWIG HILGER & MICHAEL BECHT

Catholic University of Eichstaett-Ingolstadt; Ostenstr. 18, 85072 Eichstaett, Austria
florian.haas@ku.de

Abstract In August 2011, a large rainstorm event triggered several slope type debris flows on the steep Little Ice Age moraine deposits of the Gepatschferner. Since high resolution ground-based LiDAR data are available for before and after the event, erosion and accumulation of the single debris flows could be quantified very accurately. Besides the quantification of the sediment yield of this event, the DEM of difference calculated from the two LiDAR epochs allows for the identification and detailed mapping of process areas of the debris flows. Using the ground-based LiDAR DEM and the mapped starting zones of the event, the process areas of the debris flows were modelled using a 2-D friction model. The model was calibrated and validated by the detailed maps of the process areas. The paper presents the first results of both the quantification and the modelling of the slope type debris flows caused by the 2011 rainstorm event.

Key words debris flows; proglacial area; ground-based LiDAR; modelling; PROSA

INTRODUCTION

Since the end of the Little Ice Age (LIA), the glaciers of the Alps have been retreating significantly (e.g. Klok & Oerlemans, 2004), creating a rapidly changing environment by exposing steep and highly erodible moraine deposits. The geomorphic development of these deposits is effected by the interaction of paraglacial processes (Church & Ryder, 1972; Ballantyne, 2002b), including fluvial activity (linear erosion and slope wash), mass movements or debris flows. Since the composition of the material (Hagg & Becht, 2000) and slope angles of moraine deposits provide perfect conditions for debris flows, they are reported as important geomorphic processes on steep and bare moraine deposits in proglacial areas (Palacios *et al.*, 1999; Curry *et al.*, 2006; Chiarle *et al.*, 2007; Barlow *et al.*, 2009). However, the role of melting permafrost in the debris flow process is contradictory, as discussed by Damm & Felderer (2008) and Sattler *et al.* (2011).

Due to their extensive process areas, the exact quantification and zonation of debris flows are very challenging and were conducted up to now by, e.g. field mapping and mapping on aerial photographs or by topographic surveys (e.g. by total stations, Becht *et al*., 2005). During the last few years, airborne and ground-based LiDAR (ALS and TLS) have become important methods for the topographic survey of geomorphic processes in alpine regions, such as mass movements (Bitelli *et al.*, 2004; Hsiao *et al*., 2004; Dewitte & Demoulin, 2005), fluvial processes (Haas & Heckmann, 2007; Haas *et al.*, 2011) or rock glaciers (Bauer *et al.*, 2003; Avian *et al*., 2009). In proglacial areas, the method was only used by Hetherington *et al.* (2005) and Milan *et al.* (2007) for quantifying fluvial processes in a proglacial river system. Because of the irregular occurrence of debris flows and the lack of suitable TLS data before a debris flow event, their geomorphic quantification was up to now only possible with ALS data (Scheidl *et al.*, 2008), or using a combination of ALS and TLS data (Bremer & Sass, 2012), and therefore usually resulted in a relatively high error margin.

The joint research project PROSA (*High resolution measurements of the morphodynamic in rapid changing PROglacial Systems of the Alps*), founded by the German Science Foundation (DFG) aims at a quantification of the sediment budget within the proglacial area of the Gepatschferner (Austrian Alps) by using both TLS and ALS data (cf. Heckmann *et al.*, 2012). The present study forms part of this joint project and deals with measuring and modelling of debris flows on the steep moraine deposits of LIA age. This paper shows the first quantification and modelling results of a debris flow event that occurred during a heavy rainstorm in August 2011, using pre- and post-event TLS data.

STUDY AREA AND THE DEBRIS FLOW EVENT IN AUGUST 2011

Study area

The PROSA project research area is located in the central Alps and comprises the hydrological catchment of the Faggenbach River, a tributary of the Gepatschspeicher Reservoir. Roughly 35% of the catchment is covered by the two glaciers, Gepatschferner and Weißseeferner, that are rapidly shrinking (Abermann *et al.*, 2009). A detailed description of the study area of the PROSA project and a detailed map of the whole catchment can be found in Heckmann *et al.* (2012).

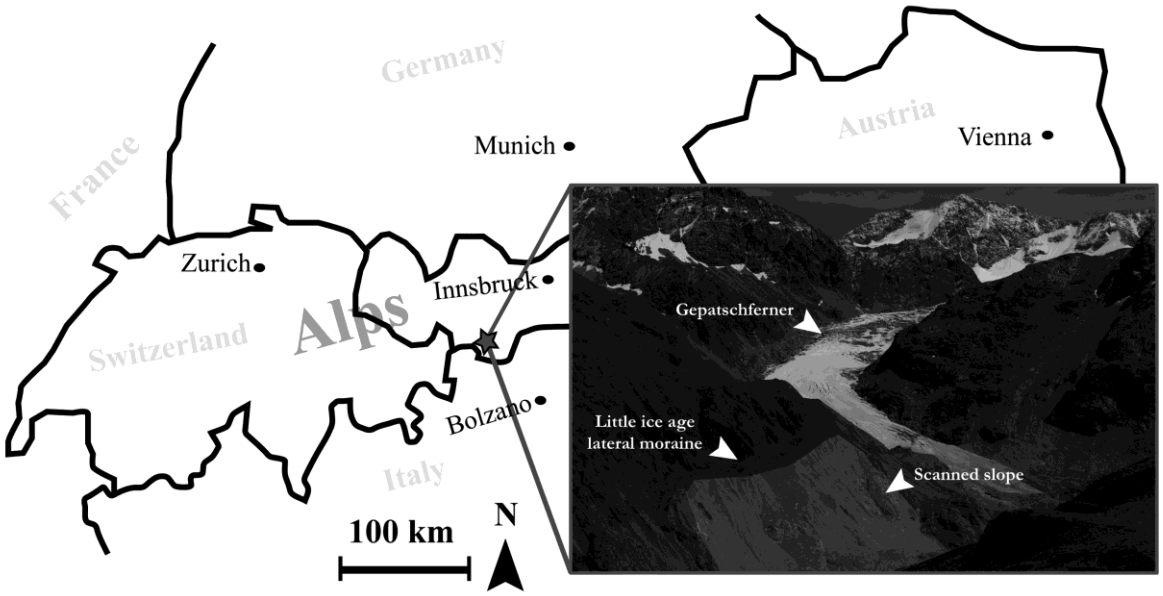

Fig. 1 Location of the study area in the central Alps of Austria. The photograph shows the Gepatschferner with its lateral moraines of the Little Ice Age and the scanned slope.

The debris flows investigated in this paper occurred on a part of the right LIA lateral moraine deposits of the Gepatschferner (Fig. 1 and Heckmann *et al.*, 2012). The scanned slope has an extent of 285 272 m^2 and a mean slope angle of 35.8° (standard deviation 12.3°). Figure 2 shows a photograph and a 3-D view (shaded relief) of the slope with its loose moraine deposits consisting of coarse to fine material (siliceous para- and orthogneiss). The slope is interspersed with rock faces and partly vegetated by alpine meadows and pioneer plants. It is clearly visible that the moraine deposits have been modified considerably by geomorphic processes since their deposition, especially by landslides, fluvial processes and debris flows. These processes have transported material from the upper to the lower parts of the slope and into the fluvial system of the Faggenbach River, which has formed a clearly visible floodplain.

Debris flow event in August 2011

During a rainstorm on 23 August 2011, intense and spatially-confined rainfall was recorded at the Weißsee pluviograph in the central part of the catchment (Morche *et al.*, 2012). The event lasted 1¾ hours and amounted to 18.8 mm with a maximal intensity of 14.4 mm h^{-1} (mean annual rainfall 800 mm). During the event, the water gauge of the Faggenbach River, close to the Gepatsch Reservoir, recorded a very high discharge with a maximum of 59.2 m^3 s^{-1} (Heckmann *et al.*, 2012; Morche *et al.*, 2012). The event triggered many slope-type debris flows in the proglacial areas within the Faggenbach catchment, especially on the steep and bare lateral moraines of the LIA. The recorded intensity fits formerly reported debris flow thresholds for the central Alps (Moser & Hohensinn, 1987; Zimmermann *et al.*, 1997). Furthermore, it was possible to attest the relationship between rainfall intensity and mean annual rainfall as described by Hagg & Becht (2000).

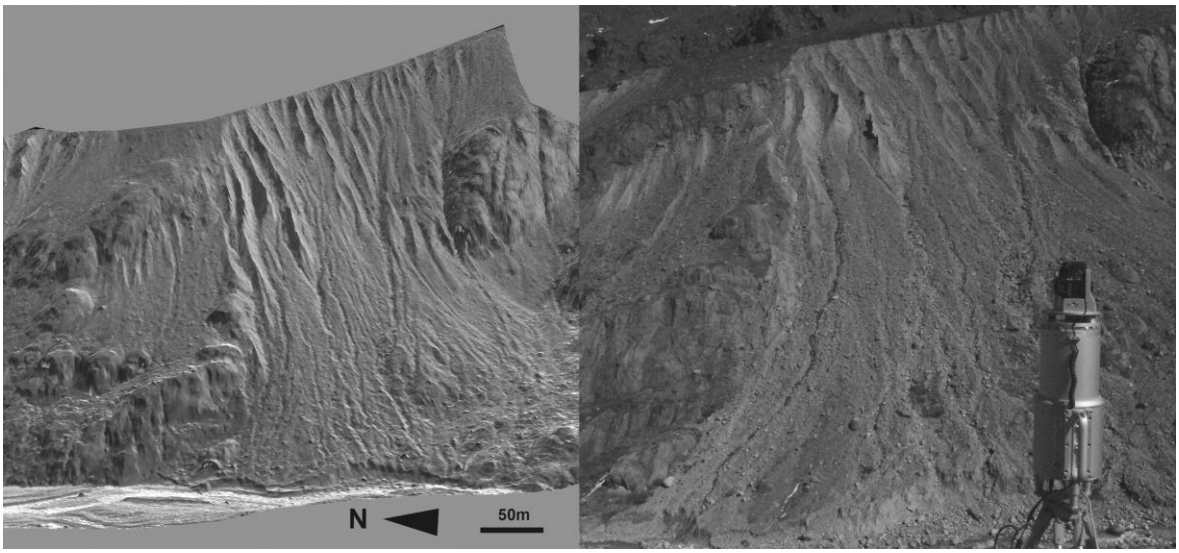

Fig. 2 Three-dimensional view (shaded relief based on the ground-based LiDAR DEM of 2011) and photograph of the scanned slope and the floodplain below.

MATERIALS AND METHODS

Scanner system

The terrestrial laser scanning system used is Riegl LMS Z420i. This long range 3-D laser scanner operates with a light in the near infrared and a beam divergence of 0.25 mrad, and can survey up to 8000 points per second to a distance of about 700 m. Data from a mounted digital SLR camera (Nikon D700) can be used to colourize the resulting point cloud. These RGB values are not only applicable for better visualization of the scanned objects, but can also be used for the filtering, e.g. of vegetated areas (Haas *et al.*, 2011). Both scanner and digital camera are operated by an external Tablet PC and the software Riscan Pro.

Data acquisition and processing

The moraine deposit slopes have been scanned twice (25.08.2010/T_1 and 24.09.2011/T_2). In order to minimize shadowing effects, the moraine deposits were scanned from three different positions (Fig. 2) by a scanning resolution of 0.05° (stepwidth of the scanning signal) for T_1 and T_2. This resulted in a mean point density of 15.7 pts m^{-2} (SD 23.9 pts m^{-2}) for the whole slope with a minimum of 0 pts m^{-2} (due to shadowing effects in the upper part of the slope) and a maximum of 534 pts m^{-2} in the scanners close-up range. The distance between the scanner and the scanned slope varies between 117 m in the lower part and 516 m in the upper parts of the slope.

The software Riscan Pro was used for the post-processing of the raw data in order to create single point clouds containing data from all three scan positions (Fig. 3). After a manual clean-up of the point clouds to eliminate "flying points" (artefacts like birds or flies), the single scan positions were spatially referenced using a two-stage procedure without the help of ground control points. First, the scan positions were matched using Riscan Pro's "coarse registration" procedure. At least four manually identified point pairs in each of the three point clouds are needed. Then, the iteratively working registration process "multi station adjustment" (MSA) of Riscan Pro was used to automatically align the point clouds based on matching planes generated from the point cloud data. Due to the expected massive geomorphic changes on the slope between T_1 and T_2, only those parts of the point clouds which belonged to immovable rock faces were used in the process. The calculated uncertainty of the MSA-registration for all adjustments varied between SD 0.019 m and SD 0.024 m.

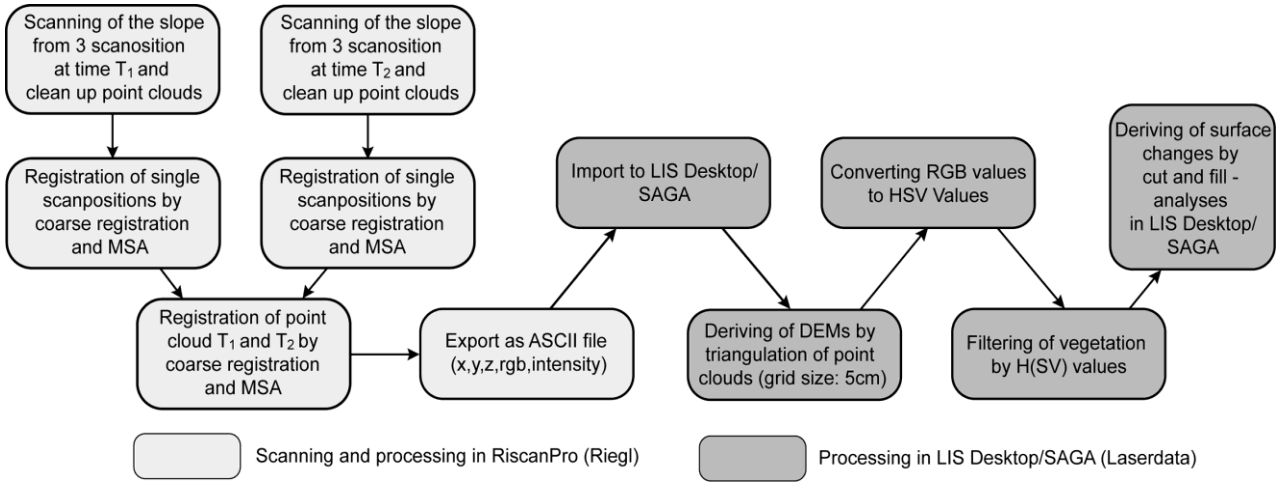

Fig. 3 Workflow of the data processing and analysing processes.

Subsequently, the point clouds (x,y,z.-coordinates and RGB values) were imported into the LIS Desktop/SAGA GIS database. To calculate the surface changes on the slope, digital elevation models with a grid size of 0.5 m (for the calculation of the surface changes) and 1.0 m (for modelling purposes) were derived from the point cloud data. Vegetation was then filtered using the colour information of every single grid cell. Colours were transformed from RGB into the HSV model and H values were used for filtering green grid cells. These were thought to represent vegetation (Haas *et al.*, 2011). By taking into account the accuracy of the measurement, the surface changes were derived by subtracting the filtered DEMs using SAGA's CutFill module (Heckmann, 2006).

Accuracy of the measurements

The uncertainty of surface change budgets based on LiDAR data is the result of many factors (Wheaton *et al.*, 2010), such as multiple signal returns due to surface roughness, the registration error, variable data quality due to measuring distance, internal precision of the measurement device or the resolution or the interpolation method, to name a few. There are many ways to account for this uncertainty (cf. Wheaton *et al.*, 2010). We calculated the error by using the "repeat surveys of unchanged surfaces" approach (Wheaton, 2008). This means that we defined the measurement accuracy of the single DEMs by scanning the slope two times with the same parameter at the same point (in September 2011). Using the two DEMs, the measurement error could then be clearly defined for each grid cell. For this test set-up a standard deviation (SD) between the two DEMs (DEM_1 and DEM_2 of September 2011) of 0.083 m was identified (n = 1 141 018 grid cells). As Brasington *et al*. (2003) described, the error of the cut and fill grid can then be defined as:

$$SD_{Cutfill} = \sqrt{(SD_{New})^2 + (SD_{Old})^2} \quad (1)$$

where $SD_{Cutfill}$ is the cut and fill grid error, and SD_{New} and SD_{Old} are the individual errors in the DEM_{New} and DEM_{Old}, respectively (cf. Wheaton *et al.*, 2010). The derived value for $SD_{Cutfill}$ is 0.1174 m. To increase the certainty of our measurement result, we defined the level of detection as $2SD_{Cutfill}$ which means that the derived error of the cut and fill grid is 0.235 m and only differences less than –2SD (–0.235 m) and greater then +2SD (+0.235 m) would be included in our volume estimation. Surface changes below this error were set to "no change" in the surface change maps.

Modelling of debris flows

Debris flows were modelled using mathematical approaches that had originally been developed to describe wet snow avalanches (Voellmy, 1955; Perla *et al.*, 1980). Wichmann (2006) combined

these concepts with a random walk and implemented them in SAGA GIS. The model, which is described in detail by Wichmann (2006), has slightly been modified and refined since 2006, including an implementation of a modified zonation rule.

The process path is modelled by a contiguous sequence of grid cells and the performance of the model is, therefore, highly dependent on DEM resolution (Wichmann *et al.,* 2008). The movement of the process itself is represented by a random walk using the grid cell centres as nodes and the directions to successor cells as edges. Because of varying topography, the system is in a different and discrete state on each of the grid cells (i.e. each position on the trajectory). Since these states are only dependent on the state on the respective next higher passed cell, the random walk used in the model qualifies as a 1-step Markov-chain. Starting at a user supplied or modelled start cell, the process path is constructed by the random walk cell-wise until a stop criterion, such as the local slope and velocity being too low, is fulfilled. The walk is confined to the directions defined by the multiple flow direction approach presented by Gamma (1996, 2000).

This approach was specifically developed for an application in random walks and identifies potential neighbouring successor cells in the DEM for the debris flow trajectories. Only neighbouring cells lower than the current cells qualify for being successor cells. In order to choose a grid cell from the set of potential successor cells, it is necessary to determine transition probabilities for potential successor cells. These are therefore calculated as proportional to their slopes. The size of the set of potential cells and their probabilities are controlled by three parameters specified by the user: slope threshold, spreading exponent and persistence factor.

The slope threshold determines the maximum slope for the start of debris flow spreading. In other words, the process more or less follows the slope line in steep areas, while in moderately steep areas (relatively to the slope threshold) neighbouring cells are included as well. This increases the tendency for spreading. Accordingly, almost all neighbouring cells are included in areas of low relief. As a result, potential lateral successor cells are found by the algorithm only within the slope interval between 0° and the slope threshold. Above the slope threshold, the process follows the line of greatest slope.

The degree of spreading in the areas less steep than the slope threshold is controlled by the spreading exponent. This involves a slope dependent weighting of potential successor cells. High values increase the tendency for the process not to follow the slope line and hence spreading.

In addition, it is possible to increase the probability that the process retains its current direction by choosing an appropriate persistence factor. Thus, abrupt changes in flow direction can be suppressed. All four parameters must be calibrated before this modelling step can be carried out.

Being multi-phase flows, debris flows have similar characteristics to snow avalanches. A rigorous physical modelling of both processes is impractical as the parameterization of these models cannot be undertaken due to the deficient data basis. Thus, the wet snow avalanche model of Voellmy (1955), enhanced by Perla *et al.* (1980), is used in our model to estimate debris flow range, velocities and process zonation. The detailed mathematical functionality of the model can be found in Wichmann & Becht (2005), Wichmann (2006) and Wichmann *et al.* (2009).

Within the model, the natural environment characteristics that influence process range in addition to slope (such as substrate and roughness of terrain surface) are accounted for by two parameters that are calibrated with the results of field work and from satellite image mapping: mass-to-drag-ratio (M/D) and Mu (μ). The mass-to-drag-ratio is a measure of the internal friction and Mu is a friction parameter for the flow–surface interface. The M/D has a high influence on the velocity of the modelled debris flow on steep slope segments, while μ is very important for velocity and range determination in flat accumulation zones.

The velocity is calculated along the process path of a single walk for every single grid cell, where the output velocity of one process path cell functions forms the input velocity of the next lower cell (Wichmann, 2006). The loss of energy due to breaks of slope from high to low is factored in by a correction of the input velocity for the next lower cell.

The calibration of the two parameters is hampered by the fact that a certain velocity on a grid cell can be obtained using different value combinations for the parameters M/D and μ. In order to be able to keep the range of possible parameter values limited, further assumptions must be made.

Most important, both parameters are assumed to be constant along the process path. As data on debris flow velocity is not available most of the time, the total run-out distance as observed in the field or mapped from remote sensing data (by ground-based LiDAR in this work) is usually used to calibrate parameter values. Being dependent on geology and particle-size distribution, both parameters must be calibrated anew in every study area, sometimes even for distinct debris flows on the same slope. Such inaccuracies are probably due to the different sized catchment areas of debris flows. An accordant negative correlation between catchment area size and μ has been reported repeatedly (Rickenmann, 1991; Zimmermann *et al.*, 1997; Gamma, 2000; Wichmann, 2006). The model also classifies the process area into erosion, transport and accumulation zones by applying a power law to define velocity and slope combination classes that define these process zones. The factor and exponent of the power law can be adjusted by the user until the modelled zonation is in accordance with the zones observed in the field.

As a single random walk gives back only one trajectory and the successor cells are chosen randomly (although in concord with their probabilities), the whole potential process area can be modelled by the successive execution of many random walks (Monte Carlo simulation). The relative frequencies of the specific grid cells being passed by a single walk are high (i.e. 100%) at the start cell and decline rapidly further down slope, especially if lateral spreading is allowed. They must not be interpreted as probabilities of occurrence because, in reality, the process paths are not determined only by topography. Therefore, it is not possible to make a binding statement about which modelled trajectories would actually be followed in a real event. However, it can be inferred in which area the trajectory will be located. The model parameters chosen for this work are described below.

RESULTS AND DISCUSSION

Quantification of debris flows

Figure 4 shows the derived surface changes on the slope between the DEMs of T_1 and T_2. Due to the long time period between T_1 and T_2, the surface changes are certainly not only the result of the debris flows that were triggered by the rainstorm event in August 2011. It is obvious that most of the negative surface changes are concentrated at the channel heads and in the channels themselves. Positive surface changes are associated with lateral channel boundaries such as levees or small debris cones, mainly on the lower part of the slope. Thus, we assume that most of the erosion and accumulation between T_1 and T_2 are the result of debris flow activity during the rainstorm.

The overall slope sediment budget (Fig. 4) of the debris flow activity of this event shows that only a small fraction of the mobilized sediments (1033.5 m^3, 29%) have been routed into the Faggenbach River and that most of the material has been deposited at levees and debris cones in lower parts of the slope (2526.8 m^3, 71%). Due to the different surface conditions of the northern and southern parts of the slope, sediment budgets are shown separately for both slopes In contrast to the southern slope, the northern slope has a slightly higher mean slope angle (60.1° SD 3.9°) and a shorter slope length. Thus, a great amount of material (59% of the eroded material) reached the main channel and only a little sediment was deposited on the slope. This indicates that this part of the slope is well coupled to the main channel. The southern part of the slope has a slightly lower mean slope angle (56.2° SD 3.9°), a longer slope length and, due to the interspersed rock faces on the southern and northern part, some natural barriers perpendicular to the line of slope. Thus, most of the eroded sediment (91%) was deposited on the slope itself (left and right parts of the slope; e.g. arrows 1 and 2 in Fig. 4) and only a small amount of material was routed into the Faggenbach River (debris flow channels in the central part of the slope, arrows 3, 4 in Fig. 4).

Beside the erosion and accumulation by debris flows described, the slope was undercut heavily by the Faggenbach River. 2749 m^3 of sediment was removed by lateral erosion of about 20 m during the event. Summarizing the sediment input by debris flow and by the lateral erosion, the slope provided 3782.5 m^3 of sediment to the main river system during the rainstorm event. The whole budget for the slope–floodplain interaction can be found in Morche *et al*. (2012).

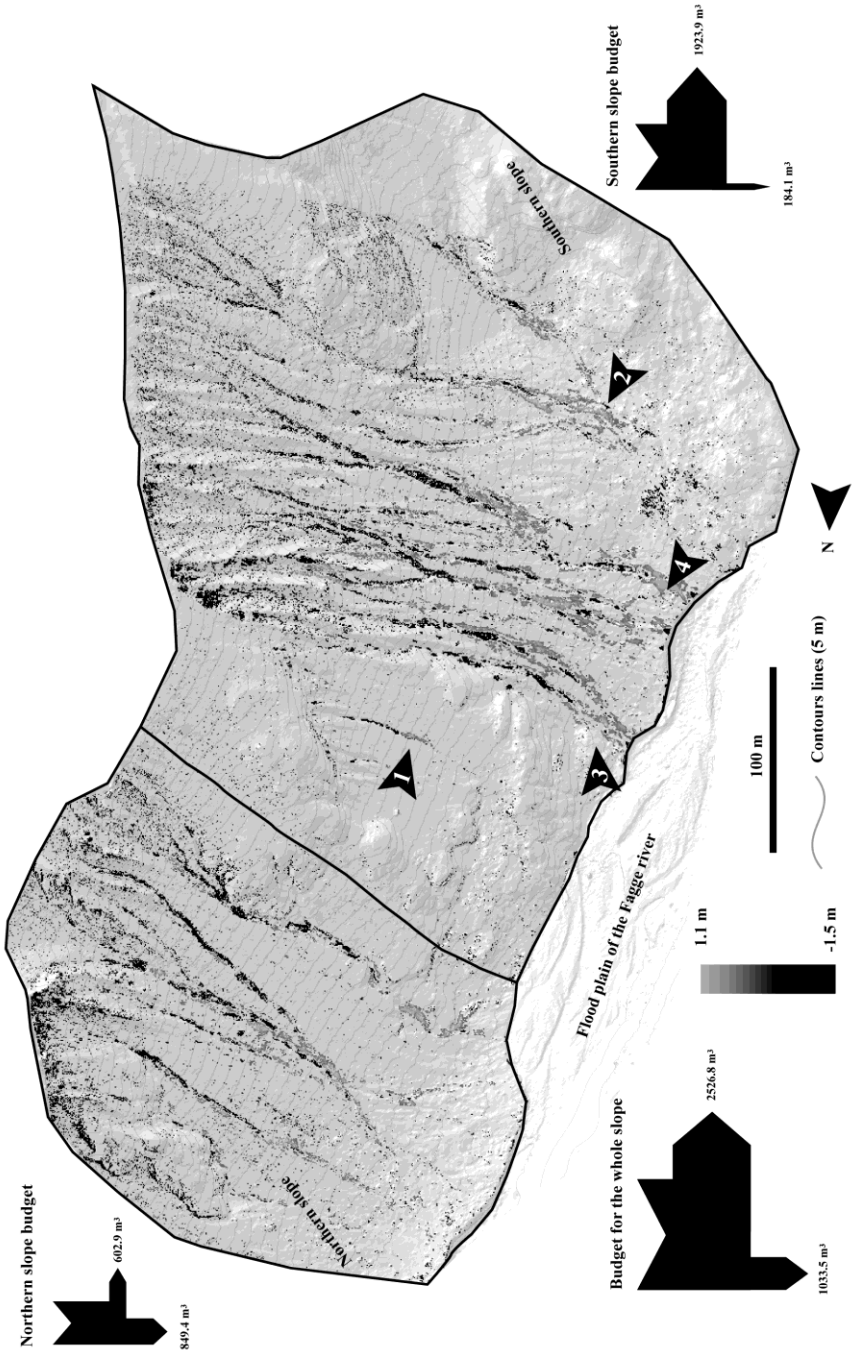

Fig. 4 Map of the surface changes on the slope and the derived sediment budget for the northern, the southern and the whole slope.

Modelling of debris flows

For this study, four debris flows on the right part of the slope were modelled using the modified model of Wichmann (2006) and a DEM with a resolution of 1 m derived from pre-event ground-based LiDAR data (August 2010). Process areas as well as erosion and accumulation zones were identified visually through the difference grid of T_1 and T_2. As a result, debris flow start grid cells could be placed manually and each of the debris flows was then modelled separately to obtain the best possible concurrence of modelled and mapped process areas. Slope thresholds were chosen according to a slope grid derived from the DEM. The spreading exponent, persistence factor and μ

were changed iteratively until optimal congruence with the mapped process areas in the difference grid was attained. The same mass-to-drag-ratio was chosen for all four debris flows. All process areas were delineated using 3000 successive random walks, and process area zonation involved the same power law for all events. The parameters used for each debris flow are given in Table 1.

Table 1 Parameter values for the single debris flows.

	Slope thres-hold	Spreading exponent	Persistence factor	M/D	μ	Zonation PL factor	Zonation PL exp-onent	No. random walks
Debris flow 1	24°	3	1.5	75	0.365	600	–1.3	3000
Debris flow 2	30°	5	5	75	0.618	600	–1.3	3000
Debris flow 3	27°	5	5	75	0.35	600	–1.3	3000
Debris flow 4	27°	5	5	75	0.35	600	–1.3	3000

As evident from Table 1, it was necessary to choose different parameters. Debris flow 2 especially seems to have involved a much higher friction at its base than the other three. This debris flow was much smaller than the other three and stopped after a travelling distance of only 37 m (Fig. 5(b)), whereas the other events travelled as far as 200 m and almost delivered a portion of their sediment to the river bed of the Faggenbach River. At least part of this enormous difference can be explained by the difference in size of the hydrological catchment areas upslope of the debris flow starting points. While debris flow 2 receives water and material only from an area of ~150 m^2, the size of the catchment areas of the other flows ranges up to >1000 m^2.

Modelling *versus* quantification

Figure 5 shows both the result of the quantification (Fig. 5(a)) and the result of the modelling of the subset of four debris flows (Fig. 5(b)) on the southern part of the slope. It is clearly visible that the modelled and the measured process areas fit quite well and that debris flow 2 has its whole

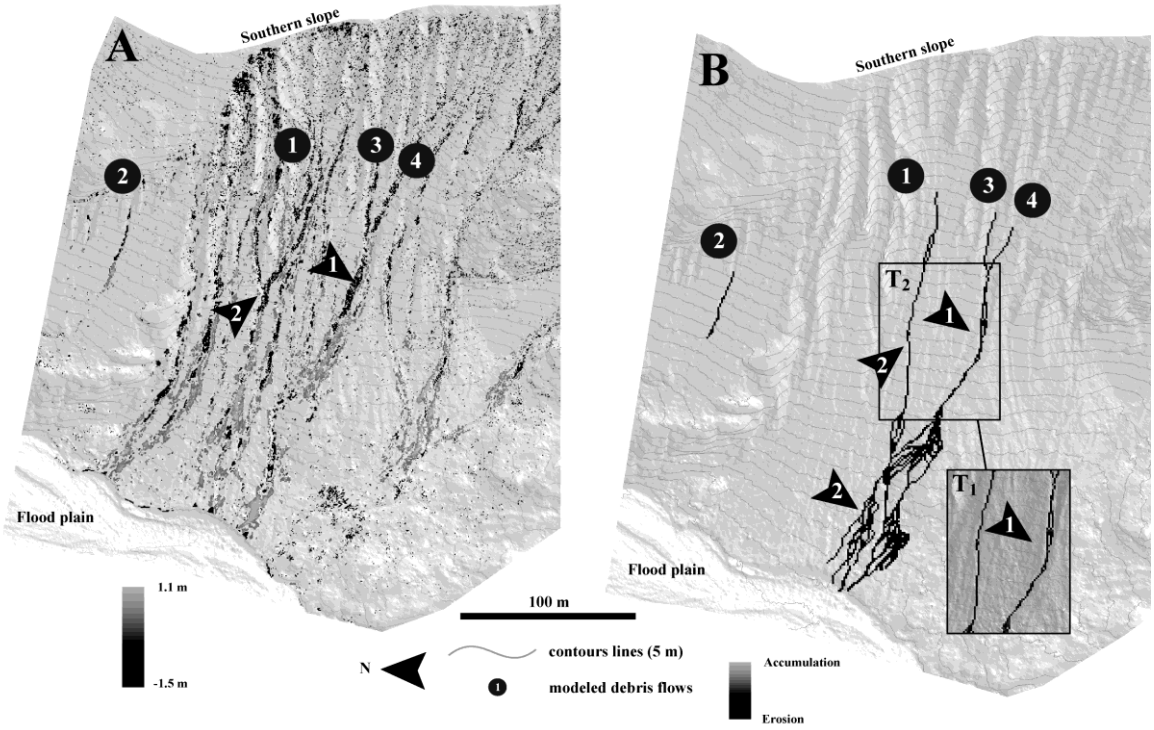

Fig. 5 Map of the surface changes on the southern slope (a), and modelled process areas of four debris flows on the southern slope, (b). The arrows in (a) and (b) indicate changes in the channel system due to erosion during the event.

process area within the slope while debris flows 1, 3 and 4 are partly connected to the Faggenbach River. This corresponds to the conditions observed on the slope. However, there are also some clearly visible differences which are indicated by arrows in Fig. 5. As the debris flows were modelled on the basis of the T_1 DEM, surface changes on the slope that occurred during the event, were not considered in the modelling process. Arrow 1, for instance, marks a zone of heavy erosion in Fig. 5(a). The modelled debris flow, however, leaves the real process path at this point as the deep erosion of the event itself is not modelled. It is probable that this direction turn had a strong influence on the run-out length and, as a consequence, also on the extent of the accumulation area. A similar case can be seen in the process path of the leftmost debris flow indicated by arrow 2. Heavy erosion in the marked channel during the event led to a process path of the debris flow completely different from the one modelled on the basis of the DEM representing the undisturbed conditions before the rainstorm event. As a result, some differences in the accumulation area extents of modelled and mapped debris flows can be made out.

CONCLUSION

The results of our case study show that ground-based LiDAR scanning is an appropriate method to quantify the surface changes of debris flows on slopes in a proglacial area. The accuracy of the measurement can be considered as quite good for the surface changes that occurred due to debris flows, but it could be improved in future by reducing the scan distance and by using targets as tie points. In order to align scans more accurately, 12 tie points have been fixed on the rock faces interspersed within the slope since our last scanning campaign. In addition, our further measurements will be carried out at a better temporal resolution in order to separate the erosion rates of single geomorphic processes and to analyse the process interactions on the slope more accurately.

Besides the quantification of debris flows, ground-based LiDAR scanning data have been shown to be applicable for improving an existing 2-D debris flow model, even though problems caused by the very detailed DEMs have to be taken into account (cf. Wichmann *et al*., 2008).

Due to the very detailed mapping, both the starting points of debris flows as well as the process zones can be well defined and this can lead to better calibration of the model. The model can be improved by more detailed mapping. It seems also be possible to use ground-based LiDAR data to derive very detailed and spatial distribution of surface roughness maps. This information can be used in the future to implement a spatially-distributed μ in the model to consider the specific surface conditions of every single debris flow.

Summing up, our investigations have shown the high potential of ground-based LiDAR scanning to investigate geomorphic processes in a proglacial environment. Further investigations in the framework of the PROSA project will help to improve these first results.

Acknowledgements This work was supported with an initial founding from the PROFOR program (program for research promotion) of the Cath. University of Eichstaett-Ingolstadt and is now founded by the German Science Foundation (DFG, BE1118/26-1). The authors also want to thank the reviewers for their helpful comments and suggestions.

REFERENCES

Abermann, J., Lambrecht, A., Fischer, A. & Kuhn, M. (2009) Quantifying changes and trends in glacier area and volume in the Austrian Ötztal Alps (1969-1997-2006). *The Cryosphere* 3, 205–215.

Avian, M., Kellerer-Pirklbauer, A. & Bauer, A. (2009) LiDAR for monitoring mass movements in permafrost environments at the cirque Hinteres Langtal, Austria, between 2000 and 2008. *Natural Hazards and Earth System Sci*ences 9, 1087–1094.

Ballantyne, C.K. (2002) Paraglacial geomorphology. *Quat. Science Reviews* 21, 1935–2017.

Barlow, J., Martin, Y. & Franklin, S., 2009. Evaluating debris slide occurrence using digital data: paraglacial activity in Chilliwack Valley, British Columbia. *Canadian J. of Earth Sciences* 46, 181–191.

Bauer, A., Paar, G. & Kaufmann, V. (2003) Terrestrial laser scanning for rock glacier monitoring. In *Permafrost: Proc. 8th Int. Conf.*) (ed. by M. Phillips, S. M. Springman & L. U. Arenson), Zurich, Switzerland, 21–25 July 2003.

Becht, M., Haas, F., Heckmann, T. & Wichmann, V. (2005) Investigating sediment cascades using field measurements and spatial modelling. *Sediment Budgets I* (ed. by D. E. Walling & A. J. Horowitz), 206–221. IAHS Publ. 291, IAHS Press.

Bitelli, G., Dubbini, M. & Zanutta, A. (2004) Terrestrial laser scanning and digital photogrammetry techniques to monitor landslide bodies. *Proceedings of the XXth ISPRS Congress, Istanbul, XXXV*, part B5, 246–251.

Brasington, J., Langham, J. & Rumsby, B. (2003) Methodological sensitivity of morphometric estimates of coarse fluvial sediment transport. *Geomorphology* 53, 299–316.

Bremer, M. & Sass, O. (2012) Combining airborne and terrestrial laser scanning for quantifying erosion and deposition by a debris flow event. *Geomorphology* 138, 49–60.

Chiarle, M., Iannotti, S., Mortara, G. & Deline, P. (2007) Recent debris flow occurrences associated with glaciers in the Alps: climate change impacts on mountain glaciers and permafrost. *Global and Planetary Change* 56, 123–136.

Church, M. & Ryder, J.M. (1972) Paraglacial sedimentation: A consideration of fluvial processes conditioned by glaciation. *Geol. Soc. Am. Bull.* 83, 3059–3071.

Curry, A.M., Cleasby, V. & Zukowskyj, P. (2006) Paraglacial response of steep, sediment-mantled slopes to post-Little Ice Age glacier recession in the central Swiss Alps. *J. Quaternary Science* 21, 211–225.

Damm, B. & Felderer, A. (2008) Identifikation und Abschätzung von Murprozessen als Folge von Gletscherrückgang und Permafrostdegradation im Naturpark Rieserferner-Ahrn (Südtirol): (Identification and assessment of debris flows as a consequence of glacier retreat and permafrost degradation in the area of Rieserferner-Ahrn, South Tyrol, in German). *Abhandlungen der Geologischen Bundesanstal* 62, 29–32.

Dewitte, O. & Demoulin, A. (2005) Morphometry and kinematics of landslides inferred from precise DTMs in West Belgium. *Natural Hazards and Earth System Sciences* 5, 259–265.

Gamma, P. (1996) Großräumige Modellierung von Gebirgsgefahren mittels rasterbasiertem Random Walk (Modeling of natural hazards in Alpine spaces by grid based random walks). In: Mandl, O., eds. Modellierung und Simulation räumlicher Systeme mit Geographischen Informationssystemen. (Modelling and simulation of spatial systems with GIS). *Proceedings-Reihe der Informatik* `96 (9), 93–105. Klagenfurt.

Gamma, P. (2000) dfwalk – Ein Murgang-Simulationsprogramm zur Gefahrenzonierung. *Geographica Bernensia* G66, 144 p. Bern.

Haas, F. & Heckmann, T. (2007) Slope Wash. In: SEDIFLUX Manual: Analysis of Source-to-Sink-Fluxes and Sediment Budgets in Changing High-Latitude and High-Altitude Cold Environments (ed. by Beylich, A. & J. Warburton). *Geological Survey of Norway publication* 2007.053 (ISSN 0800-3416), 72-75.

Haas, F., Heckmann, T., Cyffka, B. & Becht, M. (2011) Ground-based laserscanning – a new method for measuring fluvial erosion on steep slopes? In: *GRACE, Remote Sensing and Ground-based Methods in Multi-Scale Hydrology* (ed. by M. Hafeez *et al.*), 163–168, IAHS Publ. 343, IAHS Press, Wallingford, UK.

Hagg, W. & Becht, M. (2000) Einflüsse von Niederschlag und Substrat auf die Auslösung von Hangmuren in Beispielgebieten der Ostalpen (The influence of rainfall and substrate on the triggering of slope type debris flows in the eastern Alps). *Z. Geomorphol. N.F., Suppl.-Bd*. 123, 79–92.

Heckmann, T. (2006) CutFill, module for SAGA GIS.

Heckmann, T., Haas, F., Morche, D., Schmidt, K.-H., Rohn, J., Moser, M., Leopold, M., Kuhn, M., Briese, C., Pfeiffer, N. & Becht, M. (2012) Investigating an alpine proglacial sediment budget using field measurements, airborne and terrestrial LiDAR data. In: *Erosion and Sediments Yields in the Changing Environment.* IAHS Publ. 356, 438–447 (this issue).

Hetherington, David, Heritage, George & Milan, David J. (2005) Daily fine sediment dynamics on an active Alpine glacier outwash plain. In: *Sediment Budgets I* (ed. by D.E. Walling & A. J. Horowitz), 278–284, IAHS Publ. 291, IAHS Press.

Hsiao, K. H., Liu, J. K., Yu, M. F. & Tseng, Y. H. (2004) Change detection of landslide terrains using ground-based LiDAR data, in ISPRS, ed.: *Proceedings of the 2004 ISPRS Congress*.

Klok, E. & Oerlemans, J. (2004) Climate reconstructions derived from global glacier length records. *Arctic, Antarctic, and Alpine Research* 36, 575–583.

Milan, D. J., Heritage, G. & Hetherington, D. (2007) Application of a 3D laser scanner in the assessment of erosion and deposition volumes and channel change in a proglacial river. *Earth Surf. Processes Landf.* 32, 1657–1674.

Morche, D., Haas, F., Heckmann, T. & Schmidt, K. H. (2012) Sediment transport in the proglacial Fagge River (Kaunertal/Austria). In: *Erosion and Sediment Yields in the Changing Environment*. IAHS Publ. 356, 72–80 (this issue).

Moser, M. & Hohensinn, F. (1983) Geotechnical aspects of soil slips in Alpine regions. *Engng Geology* 19, 185–211.

Palacios, D., Parrilla, G. & Zamorano, J.J. (1999) Paraglacial and postglacial debris flows on a Little Ice Age terminal moraine: Jamapa Glacier, Pico de Orizaba (Mexico). *Geomorphology* 28, 95–118.

Perla, R., Cheng, T. T. & Clung, D. M. (1980) A two-parameter model of snow-avalanche motion. *J. Glaciol.* 26, 197–207.

Rickenmann, D. (1991) Modellierung von Murgängen (Modelling of debris flows). *Berichte und Forschungen Geographisches Institut Fribourg* 3, 33-45. Fribourg.

Sattler, K., Keiler, M., Zischg, A. & Schrott, L. (2011) On the connection between debris flow activity and permafrost degradation: a case study from the Schnalstal, South Tyrolean Alps, Italy. *Permafrost & Periglacial Processes* 22, 254–265.

Scheidl, C., Rickenmann, D. & Chiari, M. (2008) The use of airborne LiDAR data for the analysis of debris flow events in Switzerland. *Natural Hazards and Earth System Science* 8, 1113–1127.

Voellmy, A. (1955) Über die Zerstörungskraft von Lawinen (About the destructiveness of avalanches). *Schweizerische Bauzeitung* 73, 159-165, 212–217, 246–249, 280–285.

Wheaton, J. M., Brasington, J., Darby , S. E. & Sear, D. A (2010) Accounting for uncertainty in DEMs from repeat topographic surveys: improved sediment budgets. *Earth Surf. Processes Landf.* 35, 136–156.

Wichmann, V. & Becht, M. (2005) Modeling of geomorphic processes in an Alpine catchment. In *GeoDynamics* (ed. by P. M. Atkinson, G. M. Foody, S. E. Darby & F. Wu), 151–167. CRC Press, Boca Raton, Florida, USA.

Wichmann, V., Heckmann, T., Haas, F., Becht, M. (2009) A new modelling approach to delineate the spatial extent of alpine sediment cascades. *Geomorphology* 111, 70–78.

Wichmann, V. (2006) Modellierung geomorphologischer Prozesse in einem alpinen Einzugsgebiet - Abgrenzung und Klassifizierung der Wirkungsräume von Sturzprozessen und Muren mit einem GIS (Modelling of geomorphic processes in an alpine catchment - delineation and classification of process areas for rockfall and debris flows with a GIS, in German). *Eichstätter Geographische Arbeiten* 15, München/Wien: Profil Verlag, 231 pp.

Wichmann, V., Rutzinger, M. & Vetter, M. (2008) Digital terrain model generation from airborne laser scanning point data and the effect of grid-cell size on the simulation results of a debris flow model, *In:* Boehner, J., Blaschke, T. & Montanarella, L., eds. *SAGA - Seconds Out. (Hamburger Beiträge zur Physischen Geographie und Landschaftsökologie*, 19), 103–113.

Zimmermann, M., Mani, P. Gamma, P., Gsteiger, P., Heiniger, O. & Hunziker, G. (1997) Murganggefahr und Klimaänderung – ein GIS-basierter Ansatz (Debis flow hazard and Global Change – a GIS based approach). *Schlussbericht NFP* 31. 161 S. Zürich.